Applied Surface Science 257 (2011) 3468–3472

Contents lists available at ScienceDirect

Applied Surface Science

journal homepage: www.elsevier.com/locate/apsusc

Controlled emission from dye saturated single and coupled microcavities

V.K. Dwivedi, K. Pradeesh, G. Vijaya Prakash *

Nanophotonics Lab, Department of Physics, Indian Institute of Technology Delhi, New Delhi 110016, India

ARTICLE INFO

Article history:
Received 9 October 2010
Accepted 7 November 2010
Available online 16 November 2010

Keywords:
Optical materials
Porous silicon
Microcavity devices
Photoluminescence

ABSTRACT

Modified photoluminescence is demonstrated from the dye saturated porous silicon based single and coupled microcavities. When photonic cavity mode is weakly coupled to the emission states of the dye, photoluminescence line narrowing and intensity enhancement have been observed. Our experimental work and transfer matrix simulations and cavity modelling convincingly explain the tunability and optical field confinement within the microcavity. We also show that the photoluminescence enhancement is due to one-dimensional microcavity effect. These optically active hybrid materials from inexpensive fabrication may become an important consideration for many photonic applications.

1. Introduction

Photonic nanocomposite hybrid materials are new class of materials with many new applications, generally visualized as functional materials (e.g. semiconductor nanocrystals, organic molecules) intercalated into the interstitial spaces of a nano-dimensional host (e.g. porous materials, layered inorganics, polymer blends) [1]. Having such art of combining dissimilar components to yield improved hybrid systems have great advantage to combine distinct properties of both components into a single material. On the other hand, photonic structures, such as planar optical microcavities, are those with periodicity of modulated refractive index in the order of light-wavelength wherein the photons are conveniently confined/modulated [2]. Therefore, effective combination of hybrid materials with the photonic structures is a new class of research, of both fundamental and practical interest, having applications in advanced new-generation optoelectronic devices. In such systems, the electron–photon interactions could be either completely alter the energy states witnessing new admixture states or simply improvises the photonic features, depending on the coupling nature of photonic and electronic states [3–5]. Porous silicon (PS) has been established as most fascinating material for diverse optoelectronic applications, both for optically active (such as laser and LEDs) and passive (such as sensors) devices [6–9]. Moreover, the possibility of easily modulating its refractive index by changing the porosity, opens the way to fast, simple and inexpensive single-step fabrication of optical structures like distributed Bragg reflectors, filters and microcavities [9–12]. In general, the demonstration of enhancement/inhabitation of spontaneous emission in monolithically integrated photonic structures relies on the laborious fabrication technology, which limits the applications to specific set of materials. This limitation is due to accommodating active hosts within the structure to fully interact with the optical fields [13–15]. Therefore, porous silicon technology is the easy and inexpensive technology, especially for photonic composites where the pores can be conveniently filled with organic materials. In the recent past, organic material (dye) impregnated porous silicon composite devices were successfully fabricated and studied for emission enhancement and line narrowing in the selective wavelength region for potential applications such as biosensors [9,11,16–21].

Here we report the inexpensive fabrication and photoluminescence (PL) behaviour of photonic nanocomposite hybrid material, achieved by infiltrating an organic dye into single and coupled optical microcavities, using porous silicon technology. In single microcavity, typically one cavity photon mode with large longitudinal mode spacing lies within the stop band of the cavity. Whereas coupled microcavity has two coupled photon modes, where it comprises of two microcavities with identical optical path lengths, separated by a common distributed Bragg reflector (DBR) mirror. Coupled cavities are of particular interest to further increase the flexibility in controlling the emission as well as in the choice of selecting doubly resonant cavity wavelengths [12,14,22]. Here we demonstrate the controlled PL when the emitting energy levels of dye couple weakly to the photonic states of both single and double resonant (coupled) microcavities. Our experimental findings are compared and discussed with the theoretical results.

2. Experiment

A highly doped ⟨1 0 0⟩ oriented p^+ silicon was used for microcavity fabrication. Samples were fabricated in dark light at room

* Corresponding author. Tel.: +91 11 2659 1326; fax: +91 11 2658 1114.
E-mail address: prakash@physics.iitd.ac.in (G. Vijaya Prakash).

0169-4332/$ – see front matter © 2010 Elsevier B.V. All rights reserved.
doi:10.1016/j.apsusc.2010.11.048

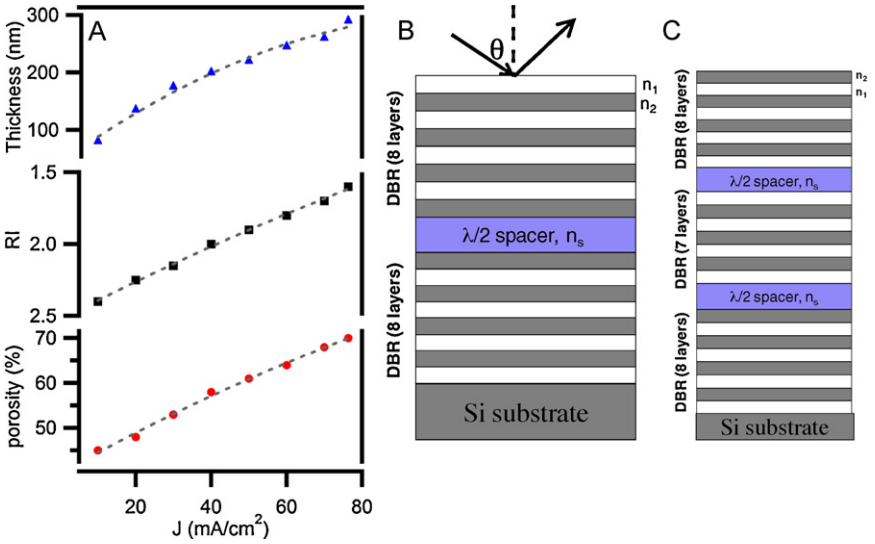

Fig. 1. (A) Plot of optimized thickness, porosities and refractive index (RI, @633 nm) for various anodisation current densities (J) of PS fabricated at 5 s duration of area 0.65 cm^2 on p^+ silicon wafer. Schematic representation of fabricated (B) single and (C) coupled PS microcavities.

temperature using a solution of HF (40%), water and ethanol mixture in the ratio of 2:1:2. Prior to the anodisation, native oxide on the surface of the silicon wafer has been conveniently removed. A potentiostat/galvanostat and a homemade Teflon cell is used, wherein a copper plate attached to the bottom of silicon wafer as anode and platinum mesh as cathode electrodes are employed for anodisation. The porosity, refractive index and the thickness of a single layer resulted as linear functions of the current density for fixed anodization time and HF concentration for a fixed doping level of the silicon wafer (Fig. 1A). The refractive index of the PS film depends on its porosity, and can be calculated in the frame of effective medium approximation (EMA), the Bruggemann model [8]. Thickness and refractive index values were obtained from single-wavelength ellipsometry (at 633 nm) and white-light reflection spectral analysis. Single and coupled microcavities were designed and fabricated for cavity mode 717 nm, as shown in the schematic Fig. 1B and C.

High (n_2 = 2.4) and low (n_1 = 1.6) refractive index PS layers corresponding to porosities 45% and 70% respectively were used. The optical thickness of alternative low and high porosity layers in the DBR is $\lambda/4$ ($=n_1d_1 = n_2d_2$, where d_1 and d_2 are corresponding thicknesses). The spacer layer is of $\lambda/2$ thick, with refractive index, n_s = 1.6 (porosity 70%). Commercial dye (LDS 751, with broad emission at 695 nm with FWHM = 65 nm) is impregnated into freshly prepared single and coupled microcavities in solution form. Concentration of the dye has been optimised to completely fill the pores of PS and the cavities were eventually dried under nitrogen flux. Angle resolved reflection and emission measurements were carried on the optical setup containing a goniometer, spectrometer and a white-light source/532 nm DPSS laser. The transfer matrix method [3] has been used to simulate the angle-dependent reflectivity spectrum and the electromagnetic field density of modes within the microcavities and compared with the experimental results.

3. Results and discussion

Fabricated single cavity contains a spacer layer of $\lambda/2$ which is sandwiched between the two distributed Bragg reflector (DBR) made up of four pairs of low and high refractive index PS layers of optical thickness $\lambda/4$ (Fig. 1B). The reflection spectra measured at 0° incident angle, of such cavity shows strong reflection dip at 717 nm, with FWHM of about 15 nm and the quality factor ($Q = \lambda/\Delta\lambda$) is estimated to be 47. The cavity is adjusted in such a way that the cavity mode is in resonance with the emission wavelength of the dye at the intermediate angles. Angle-resolved reflection spectra for both empty and dye incorporated microcavity are recorded using TE-polarized white light. Theoretical simulations are performed using transfer-matrix simulations [3], using refractive index values obtained from Fig. 1A, for the respective PS layers. The transfer-matrix simulations are in close match with the experiments (Fig. 2B). The slight mismatch can be ascribed to the non-uniformity in thicknesses/porosities, overlapping porosities at the interfaces and absorptive and dispersive nature of PS in the desired wavelength region. The cavity mode is also related to the angle of reflection by

$$E_{ph}(\theta) = E_c \times \left(\sqrt{1 - \sin^2\theta/n_{eff}^2}\right)^{-1} \quad (1)$$

where E_c = 1.73 eV (717 nm) is the cavity photon energy at normal incidence and n_{eff} (=1.95) is the effective refractive index. As seen in Fig. 2B, experimental reflection cavity mode of bare cavity (open circles) variation is matching well with simulated data (solid line). The angle resolved PL spectral image of dye impregnated microcavity is shown in Fig. 2B. As evident, the PL spectra of the dye-microcavity shows quite a narrow band with enhanced emission, tunable from 717 nm to 620 nm for the angles from 0° to 80°, follow the trend of Eq. (1). This supports the cavity effect that the weak coupling between cavity mode and the dye emission energy and the enhancement in emission is due to increased local density modes available compared to the free space.

Transfer-matrix simulations were also performed to simulate spatial image of optical field intensity inside the cavity in spectral and angle domains. As seen from Fig. 2C and D, the optical field is confined at the central spacer and also several places within the DBRs. This is particularly advantage to dye impregnated PS cavities, since the dye is uniformly distributed throughout the pores of the microcavity therefore, such redistributed optical field would contribute positively for the enhancement of the dye emission.

Dual wavelength emission from coupled microcavity is of interest for various optoelectronic applications [9,12–14]. A coupled cavity contains two microcavities separated by a common mirror. Such cavity efficiently produces two cavity modes within the photonic bandgap corresponding to the resonances of coupled microcavity. Such type of PS coupled microcavity has been designed

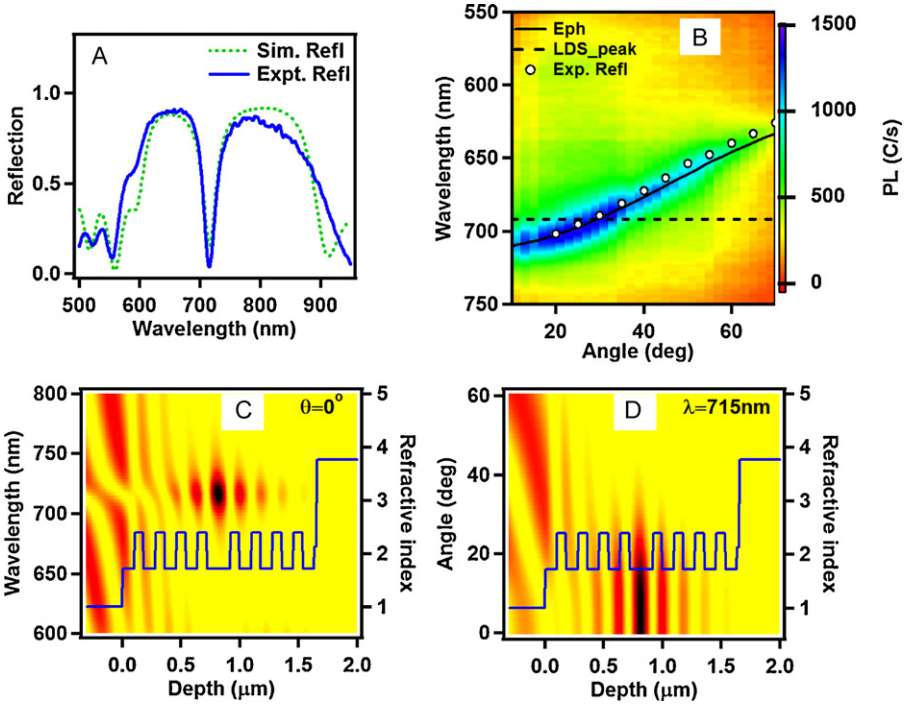

Fig. 2. (A) Experimental and transfer-matrix simulated reflection spectra of single microcavity, as shown in Fig. 1B. (B) Experimental angle dependent PL images of dye impregnated single microcavity. The open white circles represents the experimental cavity reflection dips and the solid line is from corresponding simulation. Transfer-matrix simulations of (C) spatial map of optical intensity vs. wavelength at 0° and (D) spatial map of optical intensity vs. angle at wavelength 715 nm.

as shown in Fig. 1C and fabricated. The middle DBR is designed in such a way that the reflectivity is less than both the top and bottom DBRs, to have more effective mode splitting of the two photonic modes. Fig. 3A reproduces the experimental reflection spectrum of coupled cavity along with the transfer-matrix simulated spectrum. Essentially the coupled cavity shows two photonic modes at 610 and 641 nm, designated as E_{ph1} and E_{ph2}. These are with FWHM of 13 and 15 nm with quality factor of 47 and 42 respectively. Another mode at 730 nm (E_{ph3}) within the PL region of dye is also seen, which is a leaky cavity mode. The angle resolved PL

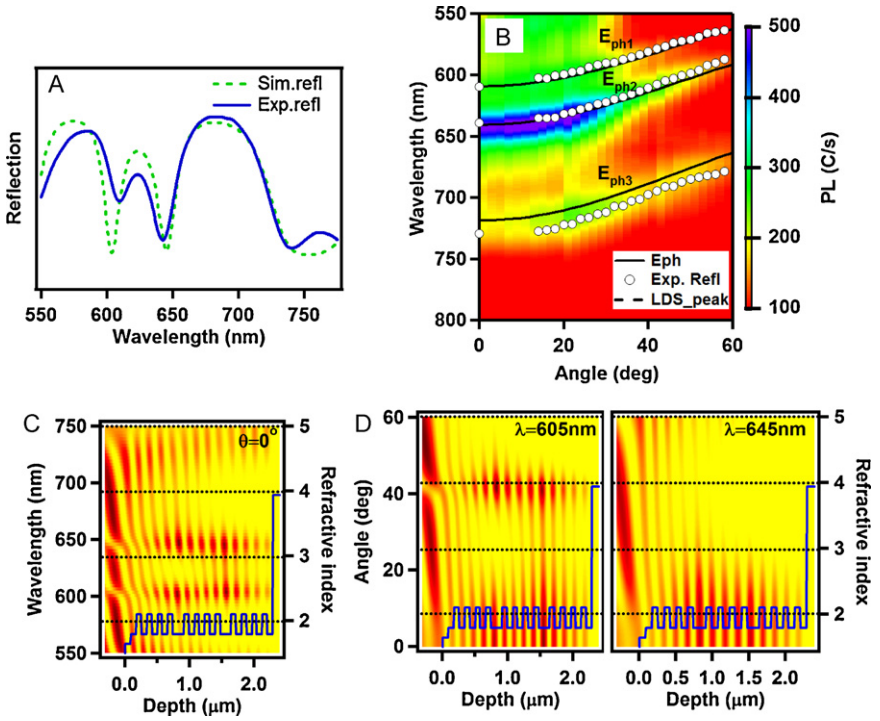

Fig. 3. (A) Experimental and transfer-matrix simulated reflection spectra of coupled cavity as shown in Fig. 1B. (B) Experimental angle dependent PL images of dye impregnated coupled microcavity. The open white circles represents the experimental cavity reflection dips and the solid line is from corresponding simulation from Eq. (1). Transfer-matrix simulations of (C) spatial map of optical intensity vs. wavelength at 0° and (D) spatial map of optical intensity vs. angle at wavelengths 605 and 645 nm, corresponding to E_{ph1} and E_{ph2} respectively.

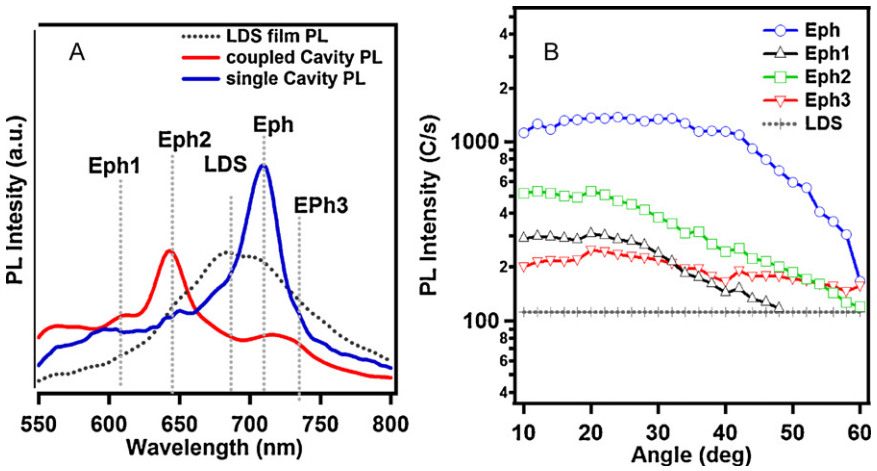

Fig. 4. (A) Experimental normalized PL spectra of dye in free space and impregnated in single and coupled cavities at normal incidence. Vertical dotted lines are to indicate the respective photonic modes of single and couple cavities. (B) Plot of PL intensity peak maxima vs. angle of dye in free-space and impregnated in single and coupled cavities for respective spectral positions, as indicated in Fig. 4A.

spectral image on dye impregnated coupled microcavity is shown in Fig. 3B. The PL spectra clearly shows three peaks, corresponding to respective photonic modes, and follow the angle tuning trend of transfer-matrix simulations and Eq. (1). Experimental reflection dips of cavity modes (white circles) along with curves (black solid lines) from Eq. (1) are also shown in the image for comparison. As seen the spectra is dominated by the narrow PL peak corresponding to E_{ph2}, obviously due to overlapping of E_{ph2} cavity mode with the dye PL peak maxima.

Transfer-matrix simulations were performed to image the spatial maps of optical field intensities inside the coupled cavity in spectral and angle domains. As seen from Fig. 3C and D, the optical field is confined equally in top and bottom spacers and also several places within the DBRs. However, the optical field is strongly confined only at lower angles for E_{ph2}, whereas for E_{ph1}, the field is distributed at 0° as well as at 40°. The ratio between the optical field intensities at PL maxima of dye in free space to the E_{ph1} and E_{ph2} are 0.06 and 0.20 suggesting more convincingly the enhanced emission at E_{ph2}.

Fig. 4A compares the normalized PL spectra recorded for dye impregnated single and coupled cavities, where PL of dye on bare substrate is also shown for comparison. When cavity modes are in resonance with the free space emission from the dye, noticeable reduction in the spectral line widths is noticed. The PL line widths are close to the FWHM of measured respective cavity modes. In addition to the sharp cavity-mode related PL, the microcavity spectra also show considerable background, corresponding to the dye emission from un-coupled region of the cavity. The PL peak intensities are plotted in Fig. 4B for single and coupled cavities, where dye emission from bare substrate is also shown. Comparatively the emission from single microcavity shows enhancement of 12 times compared to free space dye. Similarly for coupled cavity, the enhancement is 2.6 and 4.6 for E_{ph1} and E_{ph2}, respectively. This is the particular advantage in dye impregnated PS cavities, since the dye is distributed throughout the pores of cavity hence the redistributed optical field would contribute positively for the enhancement of the dye emission at various locations.

In microcavities the emission enhancement at normal incidence can be approximated [14] by

$$\frac{\Gamma}{\Gamma_0} = \frac{2F}{\sqrt{2\pi}} \frac{|E_{dye}|^2}{|E_{ph}|^2} \quad (2)$$

where F is the finesse of the cavity given by $F = \lambda_0 Q/2nd$, where Q is quality factor of the cavity mode, n is refractive index and d is thickness of spacer. E_{dye} and E_{ph} are the optical field intensities at energies of dye PL maxima and cavity mode. Considering the transfer-matrix simulations of optical field intensities (Figs. 2 and 3) and other experimental parameters, the enhancement for single cavity (E_{ph}) is estimated to be 11.3 and for coupled cavities 7.6 and 6.8 for respective E_{ph1} and E_{ph2} modes. These estimates are close to the experimental PL enhancement.

4. Conclusion

The cavity effect on photoluminescence from dye saturated porous silicon based single and coupled microcavities is demonstrated. When the photonic cavity mode is in resonance with the photoluminescence maxima of the dye, we observe narrow and enhanced PL than the dye in free-space. Transfer-matrix simulations were also performed on these microcavities and the results are convincingly supporting our experiments. These optically active hybrid materials from inexpensive and simple fabrication may become an important consideration for many photonic applications. For example, these passive photon confinement systems could be filled with electron confinement systems like semiconductor QDs or inorganic–organic nanohybrids [3,14] for strong electron–photon coupling experiments.

Acknowledgements

Authors are thankful to Dr. P. Srivastava (IIT Delhi, India) and Prof. J.J. Baumberg (Univ. of Cambridge, UK) for their help and discussions. Authors appreciate the technical help rendered by Mr. Umar Imam and Mr. Kabir Jain during the experiments. This work is part of *UK-India Education Research Initiative* (UKIERI).

References

[1] G. Kicklbick, Hybrid materials, Synthesis, characterization and applications, Willey VCH Verlag GbmH, 2007.
[2] S. Noda, M. Fujita, T. Asano, Nat. Photon. 1 (2007) 449–458.
[3] K. Pradeesh, J.J. Baumberg, G. Vijaya Prakash, Opt. Express 17 (2009) 22171–22178.
[4] H. Qiao, B. Guan, T. Böcking, M. Ga, J.J. Gooding, P.J. Reece, Appl. Phys. Lett. 96 (2010) 161106.
[5] P.G. Savvidis, J.J. Baumberg, R.M. Stevenson, M.S. Skolnick, D.M. Whittaker, J.S. Roberts, Phys. Rev. Lett. 84 (2000) 1547–1550.
[6] M.G. Berger, S. Frohnoff, W. Theiss, U. Rossow, H. Munder, Porous Silicon Science and Technology, Springer, Berlin, 1994.
[7] C.J. Oton, D. Navarro-Urrios, N.E. Capuj, M. Ghulinyan, L. Pavesi, S. González-Pérez, F. Lahoz, I.R. Martín, Appl. Phys. Lett. 89 (2006) 011107.
[8] P. Bettotti, M. Cazzanelli, L. Dal Negro, B. Danese, Z. Gaburro, C.J. Oton, G. Vijaya Prakash, L. Pavesi, J. Phys. Condens. Matter 14 (2002) 8253–8281.

[9] B. Sciacca, F. Frascella, A. Venturello, P. Rivolo, E. Descrovi, F. Giorgis, F. Geobaldo, Sens. Actuators B 137 (2009) 467–470.
[10] E. Lorenzo, C.J. Oton, N.E. Capuj, M. Ghulinyan, D. Navarro-Urrios, Z. Gaburro, L. Pavesi, Appl. Opt. 44 (2005) 5415–5421.
[11] A. Venturello, C. Ricciardi, F. Giorgis, S. Strola, G.P. Salvador, E. Garrone, F. Geobaldo, J. Non-Cryst. Solids 352 (2006) 1230–1233.
[12] L. Pavesi, G. Panzarini, L.C. Andreani, Phys. Rev. B 58 (1998) 15794–15798.
[13] P. Michler, M. Hilpert, G. Reiner, Appl. Phys. Lett. 70 (1997) 2073–2075.
[14] K. Pradeesh, G. Vijaya Prakash, J. Nanosci. Nanotechnol., in press.
[15] C.B. Poitras, M. Lipson, H. Du, M.A. Hahn, T.D. Krauss, Appl. Phys. Lett. 82 (2003) 4032–4034.
[16] Z. Deng, Y. Zhan, H. Duan, Z. Xiong, F. Bai, Y. Wang, Synth. Mat. 129 (2002) 299–302.
[17] S. Setzu, P. Solsona, S. Létant, R. Romestain, J.C. Vial, Eur. Phys. J. AP7 (1999) 59–63.
[18] S. Setzu, P. Solsona, S. Létant, R. Romestain, J.C. Vial, J. Luminesc. 80 (1999) 129–132.
[19] S. Setzu, P. Ferrand, R. Romestain, Mater. Sci. Eng. B 69–70 (2000) 34–42.
[20] S. Chan, S.R. Horner, P.M. Fauchet, B.L. Miller, J. Am. Chem. Soc. 123 (2001) 11797–11798.
[21] V. Mulloni, L. Pavesi, Appl. Phys. Lett. 76 (2000) 2523–2525.
[22] S. Stelitano, G. De Luca, S. Savasta, L. Monsù Scolaro, S. Patané, Appl. Phys. Lett. 95 (2009) 093303.